nature physics

ARTICLES

PUBLISHED ONLINE: 2 AUGUST 2009 | DOI: 10.1038/NPHYS1359

Spin-injection Hall effect in a planar photovoltaic cell

J. Wunderlich[1,2]⋆, A. C. Irvine[3], Jairo Sinova[2,4], B. G. Park[1], L. P. Zârbo[4], X. L. Xu[1], B. Kaestner[5], V. Novák[2] and T. Jungwirth[2,6]

Electrical detection of spin-polarized transport in semiconductors is one of the key prerequisites for successful incorporation of spin in semiconductor microelectronics. The present schemes are based on spin-dependent transport effects within the spin generation region in the semiconductor, or on non-local detection outside the spin-injection area using a ferromagnet attached to the semiconductor. Here, we report that polarized injection of carriers can be detected by transverse electrical signals directly along the semiconducting channel, both inside and outside the injection area, without disturbing the spin-polarized current or using magnetic elements. Our planar p–n diode microdevices enable us to demonstrate Hall effect symmetries and large magnitudes of the measured effect. Supported by microscopic calculations, we infer that the observed spin-injection Hall effect reflects spin dynamics induced by an internal spin–orbit field and is closely related to the anomalous and spin Hall effects. The spin-injection Hall effect is observed up to high temperatures and our devices represent a realization of a non-magnetic spin-photovoltaic polarimeter that directly converts polarization of light into transverse voltage signals.

Spin-polarized transport phenomena in semiconductors have been studied by a range of conventional techniques—both those used for the previous study of ferromagnets and novel approaches developed specifically for semiconductor spintronics. The techniques include magneto-optical scanning probes[1–5], spin-polarized electroluminescence[6–10] and magneto-electric measurements using spin-valve effects, magnetization dependence of non-equilibrium chemical potentials, and spin–orbit coupling phenomena[3,5,11–18]. Two of the preceding spintronic research developments have been particularly important for the observation of the spin-injection Hall effect (SIHE). First, it has been demonstrated that electrons carrying electrical current in a ferromagnet align their spins with the local direction of magnetization and that the resulting electrical signals due to the anomalous Hall effect (AHE) can be used as an alternative to magneto-optical scanning probes to measure the local magnetization[19,20]. The second group of studies have shown that an analogous spin-dependent deflection of electrons due to spin–orbit coupling that leads to the AHE is also present when unpolarized electrical currents are driven through non-magnetic semiconductors. The phenomenon is called the spin Hall effect and, unlike the AHE, yields only transverse spin and not charge imbalance[2,10]. Combining the above findings, we surmise that injecting spin-polarized electrical currents into non-magnetic semiconductors should also generate a Hall effect that, as long as the spins of the charge carriers remain coherent, yields transverse charge accumulation and is therefore detectable electrically. To observe this SIHE, we use a co-planar p–n junction device developed originally to measure the edge spin accumulation in the spin Hall effect[10,21]. The optical activity of the lateral diode is confined to a submicrometre depletion region of the p–n junction and when forward biased can sense the spin state of recombining electrons and holes through polarized electroluminescence. In the current study, we operate the diode in the reverse regime as a photocell to inject spin-polarized electrical currents into the semiconductor from a spatially confined region.

Figure 1a shows lateral micrographs of the planar two-dimensional electron–hole gas (2DEG–2DHG) photodiodes with the p-region and n-region patterned into unmasked or masked 1-μm-wide Hall bars. The effective width of individual Hall contacts is 50–100 nm and separation between two Hall crosses is 2 μm. The three-dimensional (3D) structure of samples and the experimental set-up are illustrated in Fig. 1b. The semiconductor wafer consists of a modulation p-doped AlGaAs/GaAs heterojunction on top of the structure separated by 90 nm of intrinsic GaAs from an n-doped AlGaAs/GaAs heterojunction underneath (for further details, see 'wafer 2' in ref. 22 and Supplementary Information). In the unetched part of the wafer, the top heterojunction is populated by the 2DHG, whereas the 2DEG at the bottom heterojunction is depleted. The n-side of the co-planar p–n junction is formed by removing the p-doped surface layer from a part of the wafer, which results in populating the 2DEG. At zero or reverse bias, the device is not conductive in the dark owing to charge depletion of the p–n junction. Counter-propagating electron and hole currents can be generated by illumination at subgap wavelengths. Owing to optical selection rules, the out-of-plane spin polarization of injected electrons and holes is determined by the sense and degree of the circular polarization of vertically incident light. The optical spin-injection area is controlled by bias-dependent p–n junction depletion and, additionally, by the position and focus of the laser spot or by including metallic masks on top of the Hall bars (see Supplementary Information for more details on the experimental techniques).

Figure 1c shows measurements at Hall cross H2 in the n-channel at 4 K, laser wavelength of 850 nm and for 0 and −10 V reverse bias

[1]Hitachi Cambridge Laboratory, Cambridge CB3 0HE, UK, [2]Institute of Physics ASCR, v.v.i., Cukrovarnická 10, 162 53 Praha 6, Czech Republic, [3]Microelectronics Research Centre, Cavendish Laboratory, University of Cambridge, Cambridge CB3 0HE, UK, [4]Department of Physics, Texas A&M University, College Station, Texas 77843-4242, USA, [5]Physikalisch-Technische Bundesanstalt, Bundesallee 100, 38116 Braunschweig, Germany, [6]School of Physics and Astronomy, University of Nottingham, Nottingham NG7 2RD, UK. *e-mail: jw526@cam.ac.uk.

© 2009 Macmillan Publishers Limited. All rights reserved.

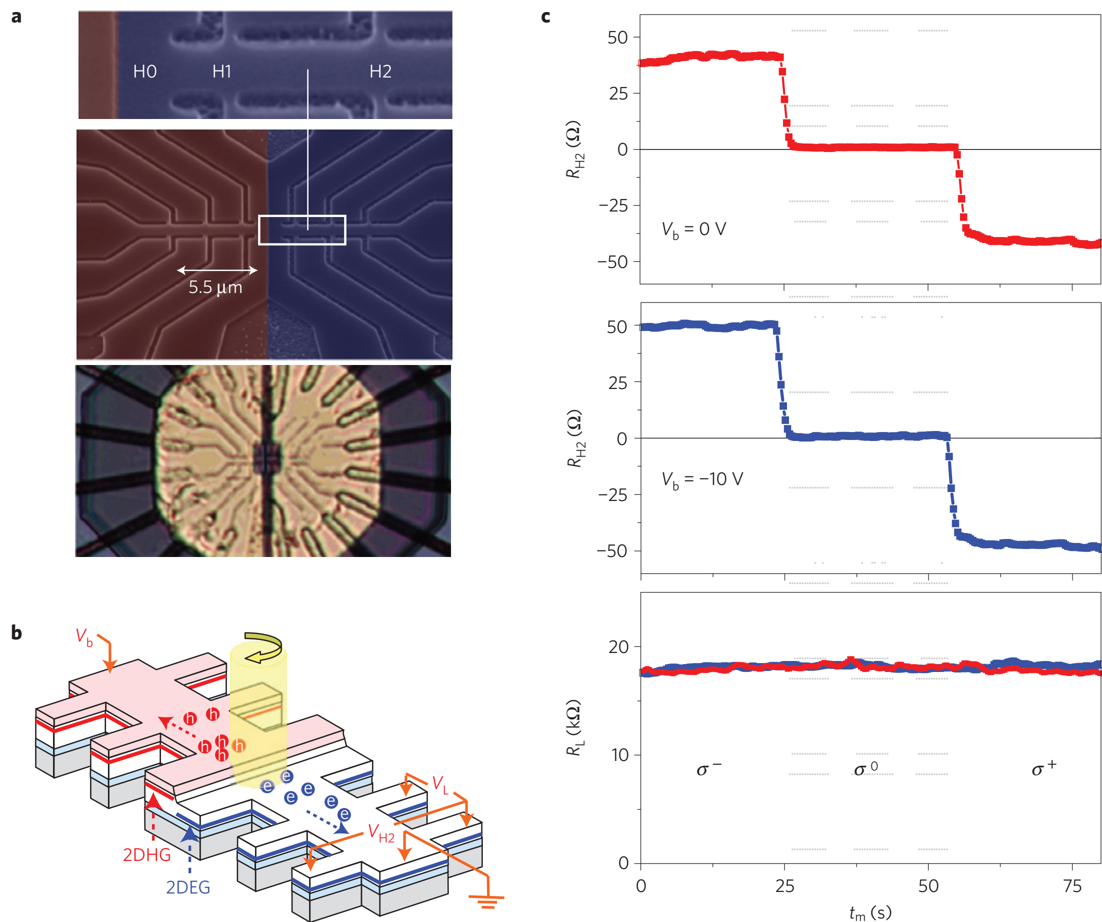

Figure 1 | Devices, schematic diagrams of the experiment and observation of the SIHE. a, Micrograph of the co-planar p–n junction device with masked Hall bars (lower panel) and images of the SIHE devices without the gold masks (upper panels). **b**, Schematic diagram of the wafer structure of the 2DEG–2DHG p–n diode and of the SIHE measurement set-up. **c**, Steady-state SIHE signals changing sign for opposite helicities (σ^- and σ^+) of the incident light beam, that is, for opposite spin polarizations of the injected electrons. For linearly polarized light (σ^0), the injected electron current is spin unpolarized and the SIHE vanishes. Measurements were carried out at the 2DEG Hall cross H2 at a laser wavelength of 850 nm, zero and reverse bias of −10 V and 4 K. Polarizations are changed electronically during the measurement by the photo-elastic modulator.

with the laser spot fixed on top of the p–n junction and focused to approximately 1 μm in diameter; ×10 larger light intensity was applied at zero bias to maintain a constant optical current of 1 μA (see Supplementary Information for more details on the measurement techniques). Whereas the longitudinal resistance R_L is insensitive to the polarization, the transverse signal R_H is observed only for polarized spin injection into the electron channel and reverses sign on reversing the polarization. In the measurements, the polarization of the incident light was controlled electronically by a photo-elastic modulator and long measurement times of the data plotted in Fig. 1c illustrate the stability of detected electrical signals. With the laser spot focused on the p–n junction, the transverse voltage is only weakly bias dependent. The large signals of tens of microvolts, corresponding to transverse resistances of tens of Ω, are detected outside the spin-injection area at a Hall cross separated by 3.5 μm from the p–n junction.

Figure 2a shows simultaneous electrical measurements at Hall cross H0, which is wider and partially overlaps with the injection area, and at remote Hall crosses H1, H2 and H3. To confirm that the transverse signals do not result from spurious effects, but originate from the polarized spin injection, we reverse in this measurement the helicity of the incident light by manually rotating a $\lambda/2$ wave plate by 45°. The signals are recalculated to Hall angles, $\alpha_H = R_H/R_L$, the magnitude of which, 10^{-3}–10^{-2}, is comparable to the AHE in conventional metal ferromagnets. The spatial variation of the sign of the transverse signals we observe is a significant feature of the SIHE. It can be explained by the combined effects of spin-dependent transverse deflection and longitudinal spin precession of electrons when propagating outside the injection area, as illustrated in Fig. 2b. We estimate the scattering mean free path in our system to be ∼10–100 nm and the typical spin–orbit coupling length to be ∼1 μm. The first length scale determines the onset of the AHE-like transverse charge accumulation due to skew scattering off spin–orbit coupled impurity potentials. The second length scale governs the spin precession about the internal spin–orbit field, which in asymmetrically confined Rashba 2DEGs tends to point in-plane and perpendicular to the electron momentum. In narrow channels, electrons injected with out-of-plane spins precess coherently about this internal spin–orbit field. The coherence can also exceed micrometre scales in wider channels owing to the extra Dresselhaus spin–orbit field originating from inversion asymmetry of GaAs, as detailed below in the theory section. Figure 2c,d shows the SIHE as a function of the degree of polarization at Hall crosses H1 and H2. Hall angles on each cross show linear dependence on the polarization of injected electrons in analogy to the linear dependence on magnetization of the AHE in a ferromagnet.

Complete Hall symmetries of the transverse signals measured in our devices are confirmed by the experiments presented in Fig. 3. Figure 3a shows data recorded in a sample with Hall crosses H2 and H3 fully covered by an insulating thin film

© 2009 Macmillan Publishers Limited. All rights reserved.

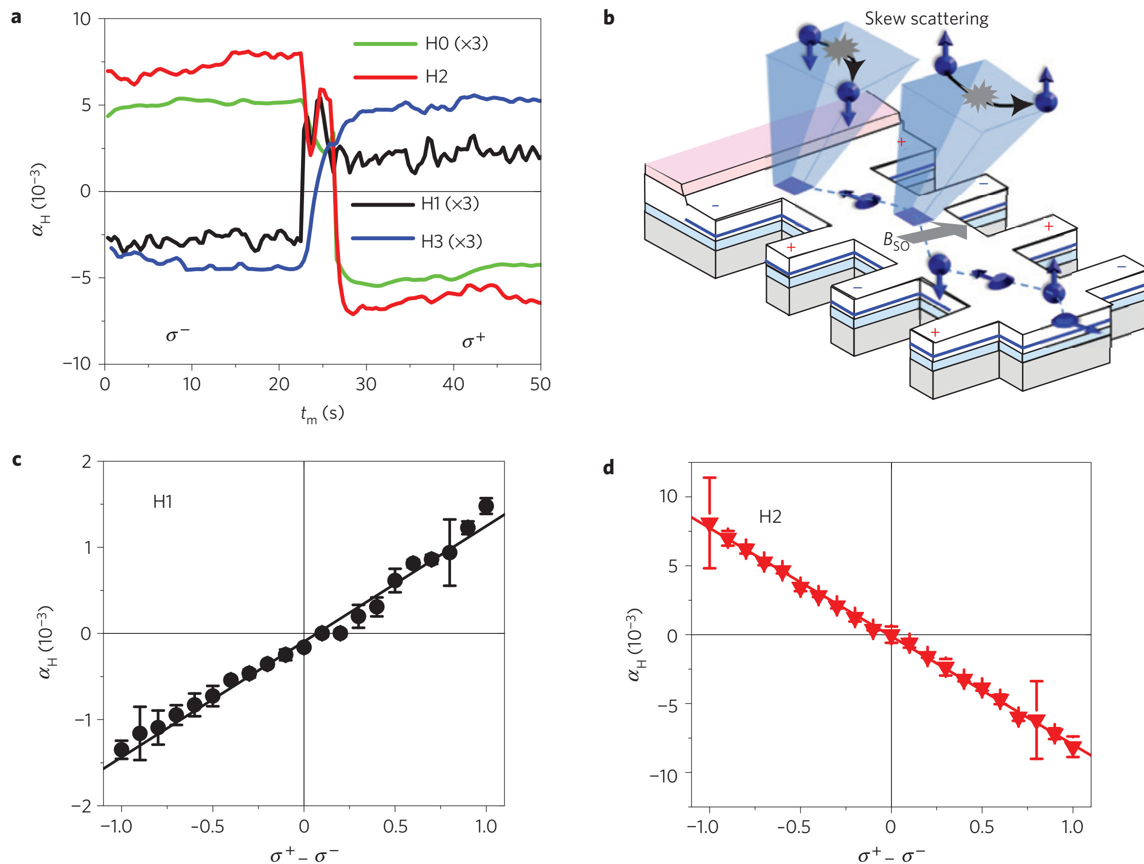

Figure 2 | Variable SIHE signals along the channel and linear dependence of the SIHE on the degree of polarization. a, SIHE signals recorded at a fixed photo-elastic modulator setting plotted for Hall crosses H0–H3 in the 2DEG channel. The grey region corresponds to the manual rotation of the $\lambda/2$ wave plate, which changes the helicity of the incident light and, therefore, the spin polarization of injected electrons. **b**, Schematic diagrams of the origin of the SIHE. Spin-polarized electrons are injected from the p–n junction into the 2DEG channel and outside the optical generation area the spins start to precess owing to the internal spin–orbit field B_{SO}. Electrical *in situ* detection of the resulting non-uniform spin polarization is enabled by the spin-dependent deflection of electrons towards the channel edges, resulting in spatially varying Hall voltages. **c**,**d**, Experimental Hall angles measured simultaneously at n-channel Hall crosses H1 and H2. The SIHE angles are linear in the degree of polarization. Each data point comprises integration over 2 min of measurement time and the error bars correspond to the maximum deviation from the average value. The laser spot is focused on the p–n junction and also the bias voltage, laser wavelength and measurement temperature are the same as in Fig. 1.

and a metallic mask. Any residual local polarization at the Hall crosses by stray light is eliminated in this sample and we again detect strong and spatially dependent signals for polarized electron injection. The SIHE is observed only at reverse bias when electrons move from the illuminated aperture towards the n-channel Hall crosses. At forward bias, optically generated electrons are accelerated in the opposite direction and we detect zero Hall signals independent of polarization.

The distinct features of the SIHE are highlighted by comparison with complementary data shown in Fig. 3b. After etching the surface layers in the n-side of the p–n diode, we were able to select wafers with residual subgap optical activity in an unmasked n-channel. We used contacts of the Hall cross H1 as the source electrode, in which case dark current flows in a bias-polarity dependent direction between H1 and the ground electrode of the n-channel. The dark current generates zero Hall voltage at crosses H2 and H3, whereas clear (albeit weak) Hall signals are detected on directly illuminating the crosses with intense circularly polarized light. The signals are attributed to the AHE because they occur inside the spin-generation area and, as expected, they are antisymmetric with respect to the current polarity. Also consistent with the AHE, we observe in these experiments Hall voltages with polarity depending only on current orientation and spin-polarization but with the same signs on all irradiated Hall crosses measured. It contrasts the SIHE measurements of spin injection from the p–n junction in which the sign can alternate among the Hall crosses. Figure 3c shows that SIHE signals can also change sign at a given Hall cross when moving the spot across the optically active region around the p–n junction, that is, when effectively shifting the spin-injection area. At large reverse biases, the optically active region extends a few micrometres deep in the p-channel. As we move the laser spot across the junction towards the p-channel, we observe simultaneous variations of the signals at both measured Hall crosses in the n-channel. The Hall voltages eventually disappear despite the presence of a still sizable optical current, suggesting that spin decoherence takes place before electrons reach the n-side of the p–n junction.

As we have Hall bars patterned also along the p-channel, we can detect another signature of spin decoherence in our electrical measurements. The character and strength of the spin–orbit coupling in the 2DHG implies coherence lengths orders of magnitude smaller than in the 2DEG channel. Consistently, no clear Hall signal is measured at the first p-channel Hall cross with the laser spot focused on top of the p–n junction. Corresponding data, presented in Fig. 4a, were taken simultaneously with the SIHE measurements at n-channel crosses H1 and H2 shown in Fig. 2c,d. Figure 4b confirms that it is the spin decoherence of propagating holes rather than an inherent absence of the Hall effect in the 2DHG that explains the negative result of measurements in Fig. 4a.

© 2009 Macmillan Publishers Limited. All rights reserved.

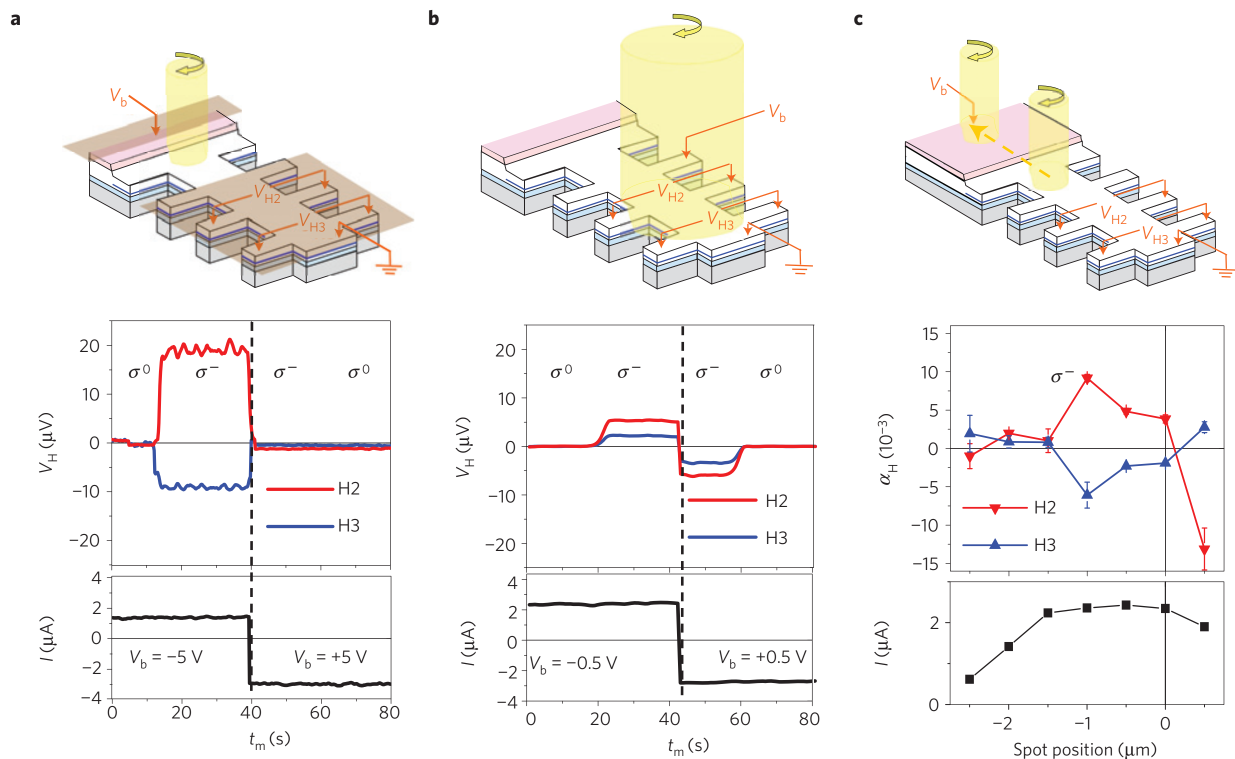

Figure 3 | Measurements of the symmetries of the Hall signals. a, SIHE measurements in a masked sample with linearly polarized light (grey regions) and circularly polarized light of a fixed helicity (white regions) for opposite polarities of the optical current. A schematic diagram of the experimental set-up is shown in the upper panel. The middle panel shows that SIHE voltages are detected only at negative bias when spin-polarized electrons move from the illuminated aperture towards the measured Hall crosses H2 and H3 in the n-channel. The optical current is plotted in the lower panel. **b**, Complementary measurements to **a** in an unmasked sample with only the n-channel biased and Hall crosses H2 and H3 directly illuminated with a ×10 stronger light intensity as compared with **a**. Weak AHE signals are detected in this case, which are antisymmetric with respect to the polarity of the current. The lower panel shows the optically generated part of the current. **c**, SIHE measurements in a −5 V reverse-biased p–n junction device with unmasked Hall bars. The spin-injection area is shifted by moving the focus of the laser spot across the junction towards the p-channel. Position '0' corresponds to the spot on top of the p–n junction. The SIHE signal at the n-channel crosses H2 and H3 changes simultaneously, at each individual cross can change magnitude and sign, and eventually vanishes when the spot is moved by several micrometres from the junction.

A strong AHE signal is detected when directly illuminating the measured p-channel Hall cross.

Finally, Fig. 5a shows measurements in a sample that showed rectifying p–n junction characteristics at temperatures up to 240 K. The data demonstrate that the SIHE is readily detectable at high temperatures. Together with the zero-bias operation shown in Fig. 1c and linearity of the SIHE in the degree of circular polarization of the incident light, these characteristics represent the realization of the spin-photovoltaic effect in a non-magnetic structure and demonstrate the utility of the device as an electrical polarimeter[15]. Note that our approach is distinct from the former proposal of the spin-voltaic effect, which assumed longitudinal transport in a magnetic system[23,24].

The aim of the experimental work discussed above was to provide evidence and explore the basic phenomenology of the SIHE. For this, we designed our devices to achieve the capability of spatially confined optical injection, non-local spin detection in well-defined Hall bar structures and compatibility with the expected micrometre scale of the spin precession. Systematic and quantitative study through the SIHE of spin dynamics in semiconductor structures with variable properties is beyond the scope of this article and in our devices requires major modifications and optimizations of the epilayer growth and device fabrication. For example, a reduction of the spacing between the Hall crosses and corresponding reduction of the size of individual Hall contacts by an order of magnitude would require nanofabrication of ∼10 nm lateral features with a depth-to-width aspect ratio of 10 in our current epilayers. This is beyond the state-of-the-art limits of electron-beam lithography combined with dry etching. Bringing the 2DEG closer to the surface and also, for example, increasing its mobility by introducing larger spacer layers in the barrier material is feasible. However, it will require a series of growth optimization steps to establish the balance between the 2DEG and 2DHG populations necessary for the formation of the co-planar p–n junction after etching. Finally, we note that experiments in external magnetic fields, often seen in the studies of spin dynamics in weakly spin–orbit coupled systems, are not well suited for inspecting basic SIHE characteristics in our relatively strongly spin–orbit coupled 2DEG. Variations in the spin precession and coherence induced by the Zeeman coupling at magnetic fields $\lesssim$1 T are expected to be weak (see Supplementary Information for more details on the relevant Monte Carlo simulations). At higher magnetic fields, the SIHE signals may contain contributions from the Zeeman and quantum orbital effects of the field on the spin dynamics, which are mixed by the spin–orbit coupling. We also expect extra effects from the field-dependent characteristics of the spin-current generation in our p–n junctions[22]. The study of the complex phenomenology of our devices at high magnetic fields is beyond the scope of our initial report of the SIHE. Instead, we provide here further insight into the physics of the SIHE obtained from microscopic theory calculations at zero magnetic field.

Our theoretical approach is based on the observation that the micrometre length scale governing the spatial dependence

© 2009 Macmillan Publishers Limited. All rights reserved.

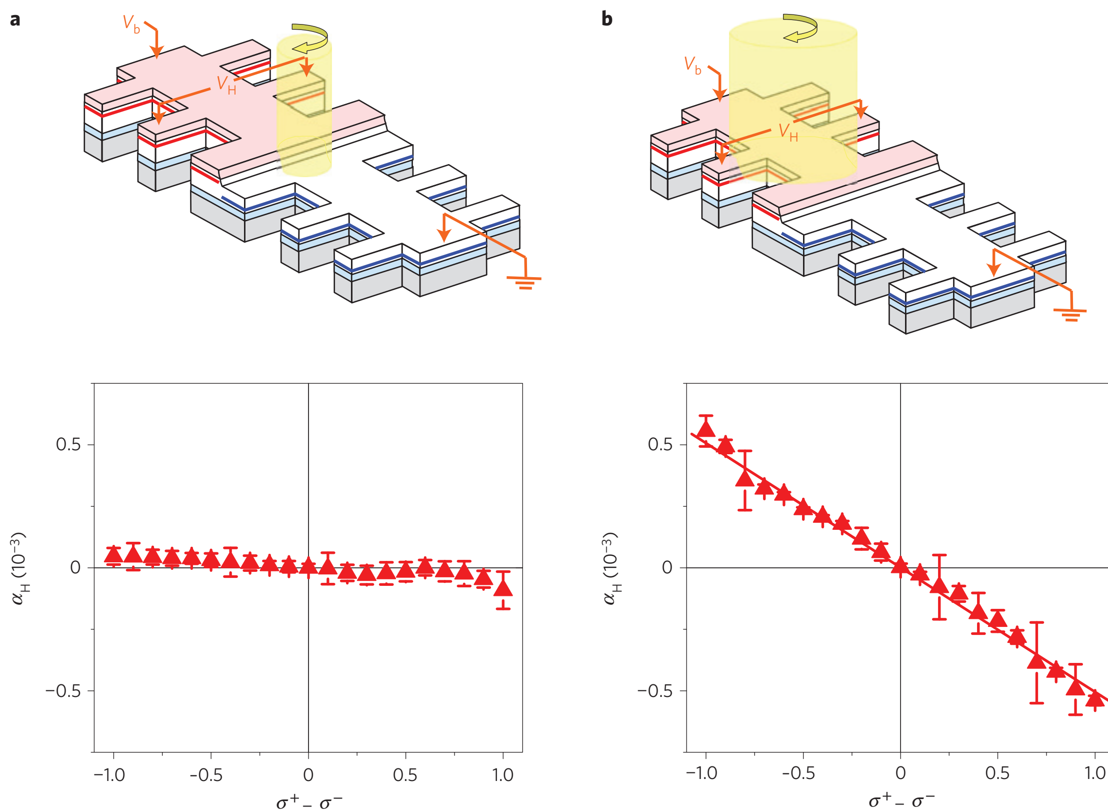

Figure 4 | Measurements on the 2DHG Hall probe. a, Data obtained for the laser spot focused on the p–n junction. **b**, Data for the spot moved on the measured 2DHG Hall cross and defocused. A measurable signal, corresponding to the AHE in a uniformly polarized 2DHG, is detected only in **b**. The error bars are determined as in Fig. 2.

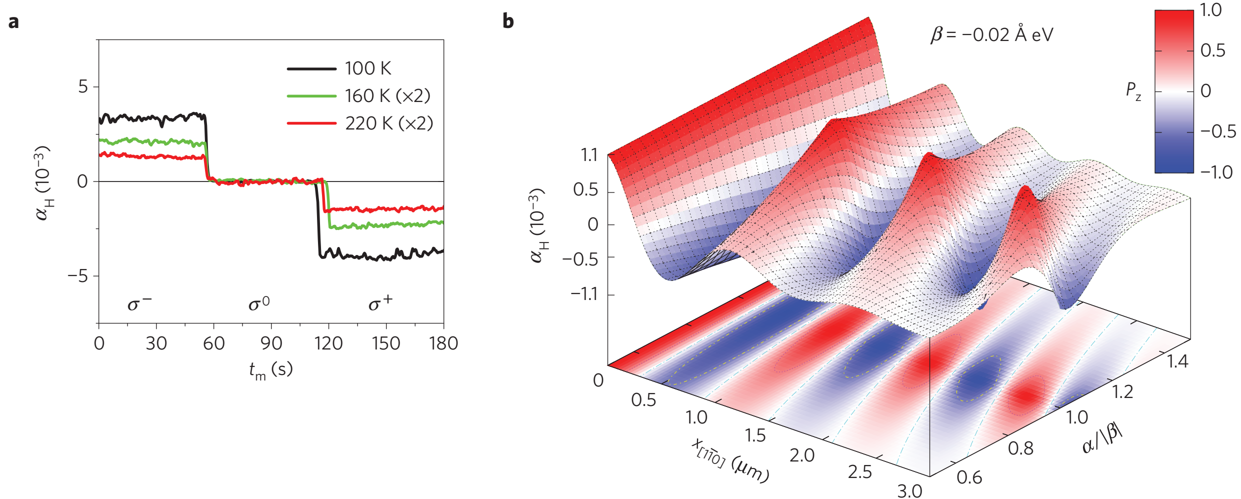

Figure 5 | Temperature dependence of the measured SIHE and theoretical modelling. a, SIHE measurements at the 2DEG Hall cross H2 at 100, 160 and 220 K. These data, together with the linear SIHE characteristics in Fig. 2c,d and zero-bias operation shown in Fig. 1c, demonstrate the realization of a transverse-voltage spin-photovoltaic effect without any magnetic elements in the structure or an applied magnetic field, and a functionality of the device as a solid-state electrical polarimeter. By choosing different semiconductor materials and heterostructures, the device can operate over a wide range of infrared and visible light wavelengths. **b**, Microscopic theory of the SIHE assuming spin–orbit coupled band-structure parameters of the experimental 2DEG system. The calculated spin-precession and spin-coherence lengths and the magnitude of the Hall angles are consistent with experiment. The colour-coded surface shows the proportionality between the Hall angle and the out-of-plane component of the spin polarization.

of the non-equilibrium spin polarization is much larger than the ∼10–100 nm mean free path in our 2DEG that governs the transport coefficients. This enables us to first calculate the steady-state spin-polarization profile along the channel and then consider the SIHE as a response to the local out-of-plane component of the polarization (see also Supplementary Information for detailed theory derivations). The calculations start from the electronic structure of GaAs, for which the conduction band near the Γ-point is formed dominantly by Ga *s*-orbitals. This implies that spin–orbit coupling originates from the mixing of the valence-band *p*-orbitals

© 2009 Macmillan Publishers Limited. All rights reserved.

and from the broken inversion symmetry in the zincblende lattice. In the presence of an electric potential $V(\mathbf{r})$, the corresponding 3D spin–orbit coupling Hamiltonian reads

$$H_{\text{3D-SO}} = [\lambda^* \boldsymbol{\sigma} \cdot (\mathbf{k} \times \nabla V(\mathbf{r}))] + [\mathcal{B} k_x (k_y^2 - k_z^2) \sigma_x + \text{cyclic permutations}] \quad (1)$$

where $\boldsymbol{\sigma}$ are the Pauli spin matrices, $\mathbf{k}$ is the momentum of the electron, $\mathcal{B} \approx 10\,\text{eV}\,\text{Å}^3$ and $\lambda^* = 5.3\,\text{Å}^2$ for GaAs (refs 25, 26). Equation (1) together with the 2DEG confinement yields an effective 2D Rashba and Dresselhaus spin–orbit coupled Hamiltonian[27,28],

$$H_{\text{2DEG}} = \frac{\hbar^2 k^2}{2m} + \alpha (k_y \sigma_x - k_x \sigma_y) + \beta (k_x \sigma_x - k_y \sigma_y)$$

where $m = 0.067 m_e$, $\beta = -\mathcal{B} \langle k_z^2 \rangle \approx -0.02\,\text{eV}\,\text{Å}$; and $\alpha = e\lambda^* E_z \approx 0.01$–$0.03\,\text{eV}\,\text{Å}$; for the strength of the confining electric field, $eE_z \approx 2$–$5 \times 10^{-3}\,\text{eV}\,\text{Å}^{-1}$, obtained from a self-consistent Poisson–Schrödinger simulation of the conduction band profile of our GaAs/AlGaAs heterostructure[10,22].

In the strong scattering regime of our structure with αk_F and $\beta k_F \sim 0.5\,\text{meV}$ much smaller than the disorder scattering rate $\hbar/\tau \sim 5\,\text{meV}$, the system obeys a set of spin-charge diffusion equations[28]. (Here, k_F is the Fermi wave vector.) In the steady state, we obtain that the spatial dependence of the out-of-plane component of the spin polarization along the $[1\bar{1}0]$ direction of our 2DEG channel is given by a damped oscillatory function $p_z(x_{[1\bar{1}0]}) = \exp(q x_{[1\bar{1}0]})$ with the complex wave vector $q = |q| \exp(i\theta)$, where $|q| = (\tilde{L}_1^2 \tilde{L}_2^2 + \tilde{L}_2^4)^{1/4}$, $\theta = (1/2) \arctan((\sqrt{2\tilde{L}_1^2 \tilde{L}_2^2 - \tilde{L}_1^4/4})/(\tilde{L}_2^2 - \tilde{L}_1^2/2))$, and $\tilde{L}_{1/2} = 2m|\alpha \pm \beta|/\hbar^2$. We note that Monte Carlo simulations including temperature broadening of the quasiparticle states confirm the validity of the above analytical results up to the high temperatures used in the experiment in Fig. 5a.

From the known local spin polarization, we calculate the Hall signal by realizing that the dominant contribution in the strong disorder regime is the extrinsic skew scattering. This contribution is obtained by considering asymmetric scattering from a spin–orbit coupled impurity potential originating from the first term in equation (1) (refs 29, 30). Within the second-order Born approximation for short-range scatterers, we obtain the spatially dependent SIHE angle[29,30],

$$\alpha_H(x_{[1\bar{1}0]}) = 2\pi \lambda^* \sqrt{\frac{e}{\hbar n_i \mu}}\, n\, p_z(x_{[1\bar{1}0]})$$

where n is the density of optically injected carriers into the 2DEG channel. Figure 5b shows the resulting theoretical α_H along the $[1\bar{1}0]$ direction for the relevant range of Rashba and Dresselhaus parameters corresponding to our experimental structure. We have assumed a donor impurity density n_i of the order of the equilibrium density $n_{\text{2DEG}} = 2.5 \times 10^{11}\,\text{cm}^{-2}$ of the 2DEG in the dark, which is an upper bound for the strength of the impurity scattering in our modulation-doped heterostructure and, therefore, a lower bound for the Hall angle. For the mobility of the injected electrons in the 2DEG channel, we considered the experimental value determined from ordinary Hall measurements without illumination, $\mu = 3 \times 10^3\,\text{cm}^2\,\text{V}^{-1}\,\text{s}^{-1}$. The density of photoexcited carriers of $n \approx 2 \times 10^{11}\,\text{cm}^{-2}$ was obtained from the measured longitudinal resistance between successive Hall probes under illumination assuming constant mobility.

The theory results shown in Fig. 5b provide a semi-quantitative account of the magnitude of the observed SIHE angle ($\sim 10^{-3}$) and explain the linear dependence of the SIHE on the degree of spin polarization of injected carriers. The calculations are also consistent with the experimentally inferred precession length of the order of a micrometre and the spin-coherence exceeding micrometre length scales. We emphasize that the 2DEG in the strong disorder, weak spin–orbit coupling regime realized in our experimental structures is a particularly favourable system for theoretically establishing the presence of the SIHE. In this regime and for the simple band structure of the archetypal 2DEG, the spin-diffusion equations and the leading skew-scattering mechanism of the spin–orbit-coupling-induced Hall effect are well understood areas of the physics of quantum-relativistic spin-charge dynamics.

The possibility to observe the SIHE in non-magnetic semiconductors, presented in our work, and to tune independently the strengths of disorder and spin–orbit coupling in semiconductor structures opens new opportunities for resolving long-standing debates on the nature of spin-charge dynamics in the intriguing strong spin–orbit coupling, weak disorder regime[31]. (For further details on the Hall effects in this regime, see Supplementary Information.) We also point out that the spatial resolution of the SIHE spin detectors, limited by the nanofabrication capabilities, is 1–2 orders of magnitude higher than the resolution of current magneto-optical scanning probes. From the application perspective, the SIHE devices can be directly implemented as spin-photovoltaic cells and polarimeters, switches, invertors, and owing to the non-destructive nature of the SIHE also as interconnects. We also foresee application of the SIHE in the Datta–Das[32] and other proposed spintronic transistor concepts[33]. Devices using the SIHE can be fabricated in a broad range of materials including indirect-gap Si/Ge semiconductors in which applicability of optical methods is limited[34]. As the magnitude of the SIHE scales linearly with the spin–orbit coupling strength, we expect $\sim\times 100$ weaker signals in the Si/Ge 2DEGs as compared with our measurements in the GaAs/AlGaAs, which is still readily detectable.

Received 19 November 2008; accepted 1 July 2009; published online 2 August 2009

References

1. Kikkawa, J. M. & Awschalom, D. D. Lateral drag of spin coherence in gallium arsenide. *Nature* **397,** 139–141 (1999).
2. Kato, Y. K., Myers, R. C., Gossard, A. C. & Awschalom, D. D. Observation of the spin Hall effect in semiconductors. *Science* **306,** 1910–1913 (2004).
3. Crooker, S. A. *et al.* Imaging spin transport in lateral ferromagnet/semiconductor structures. *Science* **309,** 2191–2195 (2005).
4. Weber, C. P. *et al.* Non-diffusive spin dynamics in a two-dimensional electron gas. *Phys. Rev. Lett.* **98,** 076604 (2007).
5. Lou, X. *et al.* Electrical detection of spin transport in lateral ferromagnet-semiconductor devices. *Nature Phys.* **3,** 197–202 (2007).
6. Fiederling, R. *et al.* Injection and detection of a spin-polarized current in a light-emitting diode. *Nature* **402,** 787–790 (1999).
7. Ohno, Y. *et al.* Electrical spin injection in a ferromagnetic semiconductor heterostructure. *Nature* **402,** 790–792 (1999).
8. Zhu, H. J. *et al.* Room-temperature spin injection from Fe into GaAs. *Phys. Rev. Lett.* **87,** 016601 (2001).
9. Jiang, X. *et al.* Highly spin-polarized room-temperature tunnel injector for semiconductor spintronics using MgO(100). *Phys. Rev. Lett.* **94,** 056601 (2005).
10. Wunderlich, J., Kaestner, B., Sinova, J. & Jungwirth, T. Experimental observation of the spin-Hall effect in a two dimensional spin–orbit coupled semiconductor system. *Phys. Rev. Lett.* **94,** 047204 (2005).
11. Chazalviel, J. N. Spin-dependent Hall effect in semiconductors. *Phys. Rev. B* **11,** 3918–3934 (1975).
12. Ohno, H., Munekata, H., Penney, T., von Molnár, S. & Chang, L. L. Magnetotransport properties of p-type (In,Mn)As diluted magnetic III–V semiconductors. *Phys. Rev. Lett.* **68,** 2664–2667 (1992).
13. Cumings, J. *et al.* Tunable anomalous Hall effect in a nonferromagnetic system. *Phys. Rev. Lett.* **96,** 196404 (2006).
14. Miah, M. I. Observation of the anomalous Hall effect in GaAs. *J. Phys. D: Appl. Phys.* **40,** 1659–1663 (2007).
15. Ganichev, S. D. *et al.* Conversion of spin into directed electric current in quantum wells. *Phys. Rev. Lett.* **86,** 4358–4361 (2001).
16. Hammar, P. R. & Johnson, M. Detection of spin-polarized electrons injected into a two-dimensional electron gas. *Phys. Rev. Lett.* **88,** 066806 (2002).

© 2009 Macmillan Publishers Limited. All rights reserved.

17. Valenzuela, S. O. & Tinkham, M. Direct electronic measurement of the spin Hall effect. *Nature* **442,** 176–179 (2006).
18. Huang, B., Monsma, D. J. & Appelbaum, I. Coherent spin transport through a 350 micron thick silicon wafer. *Phys. Rev. Lett.* **99,** 177209 (2007).
19. Wunderlich, J. *et al.* Influence of geometry on domain wall propagation in a mesoscopic wire. *IEEE Trans. Mag.* **37,** 2104–2107 (2001).
20. Yamanouchi, M., Chiba, D., Matsukura, F. & Ohno, H. Current-induced domain-wall switching in a ferromagnetic semiconductor structure. *Nature* **428,** 539–542 (2004).
21. Nomura, K. *et al.* Edge spin accumulation in semiconductor two-dimensional hole gases. *Phys. Rev. B* **72,** 245330 (2005).
22. Kaestner, B., Hasko, D. G. & Williams, D. A. Design of quasi-lateral p–n junction for optical spin-detection in low-dimensional systems. Preprint at <http://arxiv.org/abs/cond-mat/0411130> (2004).
23. Žutić, I., Fabian, J. & Sarma, S. D. Spin-polarized transport in inhomogeneous magnetic semiconductors: Theory of magnetic/nonmagnetic p–n junctions. *Phys. Rev. Lett.* **88,** 066603 (2002).
24. Kondo, T., Hayafuji, J. & Munekata, H. Investigation of spin voltaic effect in a pn heterojunction. *Jpn. J. Appl. Phys.* **45,** L663–L665 (2006).
25. Knap, W. *et al.* Weak antilocalization and spin precession in quantum wells. *Phys. Rev. B* **53,** 3912–3924 (1996).
26. Winkler, R. *Spin–Orbit Coupling Effects in Two-Dimensional Electron and Hole Systems* (Springer, 2003).
27. Schliemann, J., Egues, J. C. & Loss, D. Nonballistic spin-field-effect transistor. *Phys. Rev. Lett.* **90,** 146801 (2003).
28. Bernevig, B. A., Orenstein, J. & Zhang, S.-C. An exact SU(2) symmetry and persistent spin helix in a spin–orbit coupled system. *Phys. Rev. Lett.* **97,** 236601 (2006).
29. Nozieres, P. & Lewiner, C. A simple theory of the anomalous Hall effect in semiconductors. *J. Phys. France* **34,** 901–915 (1973).
30. Crépieux, A. & Bruno, P. Theory of the anomalous Hall effect from the Kubo formula and the Dirac equation. *Phys. Rev. B* **64,** 014416 (2001).
31. Borunda, M. *et al.* Absence of skew scattering in two-dimensional systems: Testing the origins of the anomalous Hall effect. *Phys. Rev. Lett.* **99,** 066604 (2007).
32. Datta, S. & Das, B. Electronic analog of the electro-optic modulator. *Appl. Phys. Lett.* **56,** 665–667 (1990).
33. Žutić, I., Fabian, J. & Das Sarma, S. Spintronics: Fundamentals and applications. *Rev. Mod. Phys.* **76,** 323–410 (2004).
34. Žutić, I., Fabian, J. & Erwin, S. C. Spin injection and detection in silicon. *Phys. Rev. Lett.* **97,** 026602 (2006).

Acknowledgements

We thank E. Rozkotová, Z. Výborný, V. Jurka and K. Hruška for experimental assistance, M. Borunda, A. Kovalev and S.-C. Zhang for fruitful discussions and acknowledge support from EU Grant FP7-215368 SemiSpinNet, from Czech Republic Grants FON/06/E001, FON/06/E002, AV0Z10100521, KAN400100652, LC510, and Preamium Academiae, and from US Grants ONR-N000140610122, DMR-0547875 andSWAN-NRI. J.S. is a Cottrell Scholar of Research Corporation.

Author contributions

Device fabrications: A.C.I., J.W., V.N., B.K.; experiments and data analysis: J.W., B.G.P, X.L.X., T.J., J.S.; theory: J.S., L.P.Z., T.J., J.W.; writing: T.J., J.S., J.W.; project planning: J.W., A.C.I., T.J., J.S.

Additional information

Supplementary information accompanies this paper on www.nature.com/naturephysics. Reprints and permissions information is available online at http://npg.nature.com/reprintsandpermissions. Correspondence and requests for materials should be addressed to J.W.

© 2009 Macmillan Publishers Limited. All rights reserved.